Nano Energy 61 (2019) 404–410

Contents lists available at ScienceDirect

Nano Energy

journal homepage: www.elsevier.com/locate/nanoen

Full paper

Surface-engineered mesoporous silicon microparticles as high-Coulombic-efficiency anodes for lithium-ion batteries

Jiangyan Wang[a,1], Lei Liao[a,1], Hye Ryoung Lee[a], Feifei Shi[a], William Huang[a], Jie Zhao[a], Allen Pei[a], Jing Tang[a], Xueli Zheng[a], Wei Chen[a], Yi Cui[a,b,*]

[a] Department of Materials Science and Engineering, Stanford University, Stanford, CA, 94305, USA
[b] Stanford Institute for Materials and Energy Sciences, SLAC National Accelerator Laboratory, 2575 Sand Hill Road, Menlo Park, CA, 94025, USA

ARTICLE INFO

Keywords:
Silicon anode
Surface-engineering
Mesoporous microparticle
Coulombic efficiency
Lithium-ion battery

ABSTRACT

High-capacity silicon anodes suffer from rapid capacity decay due to large volume expansion, which causes mechanical fracture, electrical contact loss and unstable solid electrolyte interphase (SEI). Nanostructuring has proved to be effective in addressing these problems over the past decade; however, new issues such as poor initial Coulombic efficiencies due to increased surface area remain unsolved. Here we develop a surface-engineering strategy by depositing a dense silicon skin onto each mesoporous silicon microparticle and further encapsulating it with a conformal graphene cage, which improves both the initial and later-cycle Coulombic efficiencies. The silicon skin lowers the unfavorable electrolyte/electrode contact area and minimizes SEI formation, resulting in an initial Coulombic efficiency over twice as high as that without silicon skin coating. The graphene cage combined with the inner void space of mesoporous silicon allow for silicon expansion, which guarantees structural integrity and SEI stability, resulting in high later-cycle Coulombic efficiencies (99.8–100% for later cycles) and impressive cycling stability.

1. Introduction

Silicon (Si), with a rich natural abundance and 10 times higher theoretical specific capacity than the state-of-the-art graphite anode, is considered as one of the most promising anode materials for the next-generation lithium-ion batteries (LIBs) [1–5]. However, silicon suffers from rapid capacity decay caused by the large volume expansion (~300%) during battery operation, which induces mechanical fracture, solid electrolyte interphase (SEI) failure, and loss of interparticle electrical contact [6,7].

In order to address these limitations, new material designs for Si anodes have been proposed. Typically, given that fracture toughness is highly improved when the material size is decreased to the nanoscale, various nanostructures have been developed. For example, Si nanowires [8] or core-shell Si nanowires such as Si/SiO_2 [9] and Si/$TiSi_2$ [10] with high aspect ratios have been fabricated through chemical vapor deposition (CVD) method for stable LIB anode materials. Besides, Si nanorods [11,12], nanoporous Si [13–15], and Si—C composites [16–18] have also received extensive considerations. In addition, the design of an interior void space also shows great promise to accommodate volume expansion. Hollow Si particles [19], tubes [20,21], yolk-shell Si@void@C [22,23] and pomegranate structures [24] have been synthesized through templating method to effectively improve the cycling stability. Despite the impressive improvements achieved by these two concepts, new challenges were introduced: high-cost for the synthesis of nanostructured Si, and poor initial and/or later-cycle Coulombic efficiencies. Recent work on non-filling C—Si structures [25] shows an improved later-cycle Coulombic efficiency, but remain inhibited by low initial Coulombic efficiency (ICE) as a consequence of the large surface area and irreversible trapping of Li by the dangling bonds of the amorphous carbon coating.

Here, we demonstrate a surface-engineered Si mesoporous microparticle to significantly improve both the initial and later-cycle Coulombic efficiencies. Mesoporous Si microparticles are obtained by thermal disproportionation of low-cost SiO microparticles and subsequent removal of the SiO_2 by-product; the mesoporous Si microparticle is then coated by a Si skin and encapsulated with a graphene cage. Such a design offers multiple attractive advantages: (1) The Si skin prevents the electrolyte from diffusing into the interior and restricts SEI formation to the outer surface (Fig. 1), thus resulting in a highly improved initial Coulombic efficiency (Table 1, 37.6%, 87.5%, before and after Si skin coating); (2) the non-filling Si skin retains

* Corresponding author. Department of Materials Science and Engineering, Stanford University, Stanford, CA, 94305, USA.
E-mail address: yicui@stanford.edu (Y. Cui).
[1] These authors contributed equally to this work.

https://doi.org/10.1016/j.nanoen.2019.04.070
Received 25 October 2018; Received in revised form 26 January 2019; Accepted 18 April 2019
Available online 25 April 2019

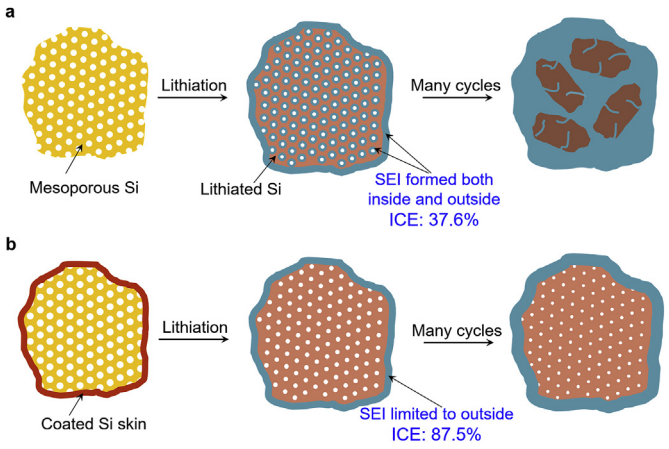

Fig. 1. Design of Si skin coating on mesoporous Si microparticles. a, Without Si skin coating, electrolyte diffuses into the inner pores, resulting in excessive SEI formation both inside and outside, and low initial Coulombic efficiency (ICE) of 37.6%. **b,** after Si skin coating, electrolyte is prevented from diffusing into the interior space, thus restricting SEI formation to the outer surface, and highly improved ICE of 87.5%.

internal void space to accommodate the volume expansion, thus guaranteeing good cycling stability; (3) the graphene cage's intrinsic high electronic conductivity and ionic permeability endow Si microparticles with an electrochemically active surface; (4) the SEI is expected to form mainly on the mechanically strong and flexible graphene cage, inducing stable SEI formation and resulting in improved later-cycle Coulombic efficiencies; (5) SiO microparticles are commercially available and inexpensive, making the anode material cost-effective and scalable.

2. Material fabrication and characterization

The synthesis process of our surface-engineered mesoporous Si microparticles is shown clearly in Fig. 2a. Commercially available SiO particles (~325 mesh) (Fig. S1) were first ball-milled to decrease the size to 1–6 μm (Fig. S2). These SiO particles were then annealed at 950 °C under Ar atmosphere (named SiO-950). During the annealing process, the thermal disproportionation of SiO and subsequent phase separation forms a microparticle of interconnected Si nanoparticles (NPs) embedded in a SiO_2 matrix [15,26]. After removing the SiO_2 matrix with HF solution, mesoporous Si (Mp-Si) microparticles were obtained. A dense Si skin was then deposited onto each Mp-Si microparticle through chemical vapor deposition, resulting in Si sealed mesoporous Si (Mp-Si@Si) microparticles. These Mp-Si@Si microparticles were further encapsulated by highly conformal graphene cages through an electroless deposition of Ni catalyst (also a template for providing void space) followed by CVD growth of graphene via a dissolution precipitation mechanism [23,27–29] at low temperature (450 °C). Finally, the Ni catalyst was etched away using $FeCl_3$ aqueous solution, resulting in graphene cage-encapsulated Si skin-sealed mesoporous Si (Mp-Si@Si@G) microparticles.

Representative transmission electron microscopy (TEM) and scanning electron microscopy (SEM) images of the product obtained at different steps in the synthesis process are shown in Fig. 2b-m. The heat-treated SiO microparticles have sizes of 1–6 μm and smooth surfaces as shown in the inset SEM images (Fig. 2b). The interconnection of sub-10nm Si NPs embedded in a SiO_2 matrix can be obviously observed from the TEM (Fig. 2i) and high-resolution TEM (HRTEM) images (Fig. S3). The distinct lattice fringes with a d-spacing of 3.2 Å (111) indicate the crystalline nature of Si NPs, whereas the neighboring amorphous material is SiO_2. X-ray diffraction (XRD) characterization further verified that the SiO microparticles converted to nanocrystalline Si with an average size of ~8 nm (estimated by the Debye–Scherrer equation) and amorphous SiO_2 (Fig. 2j) after annealing, which agrees well with the HRTEM results. X-ray photoelectron spectroscopy (XPS) (Fig. S4) also shows the coexistence of Si and SiO_2 in the annealed SiO particles: the peak observed at ~99 eV corresponds to the binding energy of Si(0), while the peak centered at ~ 103 eV suggests the presence of SiO_2 [22].

After the removal of SiO_2 by HF-etching, a crystalline Si framework was obtained (Fig. 2c,j,k). XRD patterns show significant suppression of the broad SiO_2 peak after HF-etching, while the remaining weak SiO_2 bump in XPS spectrum may be attributed to natural oxidation in air. The surface roughness of the microparticle increases greatly after etching as revealed by SEM (Fig. 2c), while the highly porous structure is clearly confirmed by TEM (Fig. 2g) and focused ion beam SEM (FIB-SEM) characterizations (Fig. 2k). After coating 100 nm of Si skin onto the mesoporous microparticle, the surface smoothens again (Fig. 2d). More importantly, the inner highly mesoporous structure is well retained, indicating that the Si skin only wraps the outer surface of the particles (Fig. 2l).

To further improve the electrochemical performance, the Mp-Si@Si microparticle was further encapsulated by a graphene cage (Fig. 2e,i,m). Mp-Si microparticles without a Si skin but encapsulated with a graphene cage (Mp-Si@G) were also prepared for comparison (Fig. S5). Evidently, the graphene cage exhibits a wavy structure, which is due to conformal graphene growth along the large grains of Ni deposited on the Si microparticle (Fig. S6). The highly graphitic nature of the graphene cage is demonstrated by the clearly observed multilayered structure through TEM (Fig. 2m), and further confirmed by Raman spectroscopy (Fig. S7). The characteristic Raman peak intensity ratio I_D/I_G is calculated to be around 0.98. The big I_D/I_G ratio and pronounced D band with a narrow bandwidth suggest that there are sufficient defects present in our Mp-Si@Si@G sample, which facilitates the Li^+ ion transport to Si [23]. Thermogravimetric analysis (TGA) reveals that the graphene cages make up only ~ 8% of the total mass of the Mp-Si@Si@G composite (~10% for Mp-Si@G composite) (Fig. S8). The lower carbon content compared with previous works [15,24,25] is assumed to minimize the irreversible trapping of Li ions by the graphene structure and improve Coulombic efficiency without sacrificing the specific capacity.

3. *In situ* lithiation of Mp-Si@Si@G microparticles

Sufficient internal void space is necessary to maintain the structural integrity of the Si anode. To verify the compatibility of our Mp-Si@Si@G structure with the drastic volume expansion of the Si anode, an *in situ* TEM study for the lithiation of Mp-Si@Si@G microparticles was performed and compared with the lithiation of dense Si microparticles (Fig. 3). The electrochemical cells for the *in situ* TEM study are shown schematically in Fig. 3a and c. A series of images were taken at certain intervals from a movie recording the *in situ* lithiation process of Si anodes to monitor their structure changes. An apparent volume expansion of the dense Si microparticle was observed (Fig. 3b and Supplementary Movie 1), cracks appeared after only 32s and widened with prolonging time. At 160s, the dense Si microparticle fractured violently into smaller particles. In contrast, the structural integrity of Mp-Si@Si@G microparticle is well-maintained through the whole lithiation process (Fig. 3d and Supplementary Movie 2). At 0 s (before lithiation), the surrounding graphene shell is clearly observed outside the inner Si microparticle. The Si microparticle volumetrically expands as Li ions diffuse through the outer graphene shell and alloy with Si. The full lithiation of the Si microparticle was achieved around 168s as indicated by the minor TEM contrast change of graphene shell after that point [25]. The structure remains intact even after full-lithiation, which is ascribed to the sufficient inner pore space of the Mp-Si@Si@G microparticle which can accommodate the large volume expansion, and the mechanically strong graphene cage that limits expansion of the Si core. These results indicate that our synthetic mesoporous-core@Si-skin@graphitic-cage structure can effectively prevent the Si anode from pulverization during lithiation and thus improving the cycling life of the

Table 1
Summary of specific surface area, total pore volume and lithium-ion battery performance for different products. Specific surface area was calculated from Brunauer–Emmett–Teller (BET) data from 0.05 to 0.20 using Quantum software analysis system.

Sample	Specific surface area (m^2/g)	Total pore volume (cm^3/g)	Initial Coulombic efficiency (%)	Initial lithiation capacity (mAh/g)	Initial delithiation capacity (mAh/g)	Delithiation capacity of the 300th cycle (mAh/g)
Mp-Si	229	0.28	37.6	3338	1256	–
Mp-Si@G	–	–	70.3	3218	2264	792
Mp-Si@Si	1.9	0.028	87.5	3084	2698	534
Mp-Si@Si@G	–	–	88.7	3197	2834	1246

battery.

Supplementary video related to this article can be found at https://doi.org/10.1016/j.nanoen.2019.04.070.

4. Electrochemical performance

The advantages of our Mp-Si@Si@G microparticles were further verified by electrochemical tests both in half-cell and full-cell configurations. Type 2032 coin cells were constructed for deep galvanostatic cycling tests from 0.01 to 1 V (half cell, 0.01–2.0 V for the first three activating cycles) and 3.0–4.2 V (full cell). All reported capacities are based on the total mass of Si and C in the composite.

Coulombic efficiency is one of the most important parameters to evaluate the performance of a battery, especially in the early cycles, which account for most of the Li-ion loss and electrolyte consumption during SEI formation. As shown in Fig. 4a and Table 1, the initial Coulombic efficiency of Mp-Si@Si@G microparticles is superior to any other intermediate products, reaching 88.7%. The poor ICE of Mp-Si microparticles (37.6%) is due to their large specific surface area (229 m^2/g, as shown in Table 1), which results in increased side reactions and a large amount of irreversible Li-consumption. After sealing with a dense Si skin, the specific surface area decreased to only 1.9 m^2/g and the ICE improved greatly to 87.5% owing to reduced side reactions and decreased SEI formation [30]. After further encapsulation with the graphene cage, the ICE of Mp-Si@Si@G microparticles reaches 88.7%, which is over two times as high as that of the Mp-Si microparticles. More interestingly, distinct from other high-performing nano-Si anodes which typically require many cycles to reach Coulombic efficiencies above 99% [20], the Coulombic efficiency of Mp-Si@Si@G microparticles reached an excess of 99% after only 7 cycles (Fig. 4c) and stabilized at a high level afterwards (99.8%–100%).

The improvement in both early- and later-cycle Coulombic efficiencies can be explained from two aspects: the reduced surface area by Si skin coating and graphitic nature of the graphene cage guarantee limited initial SEI formation, and the mechanically stable electrode/electrolyte interface prevents continued SEI formation [23]. Firstly, the Si skin greatly lowers the surface area accessible to electrolyte, thus minimizing side reactions and irreversible Li consumption. This can be verified by the cyclic voltammetry results (Fig. S10): for the Mp-Si sample, an obvious reduction peak at about 1.15 V corresponding to the

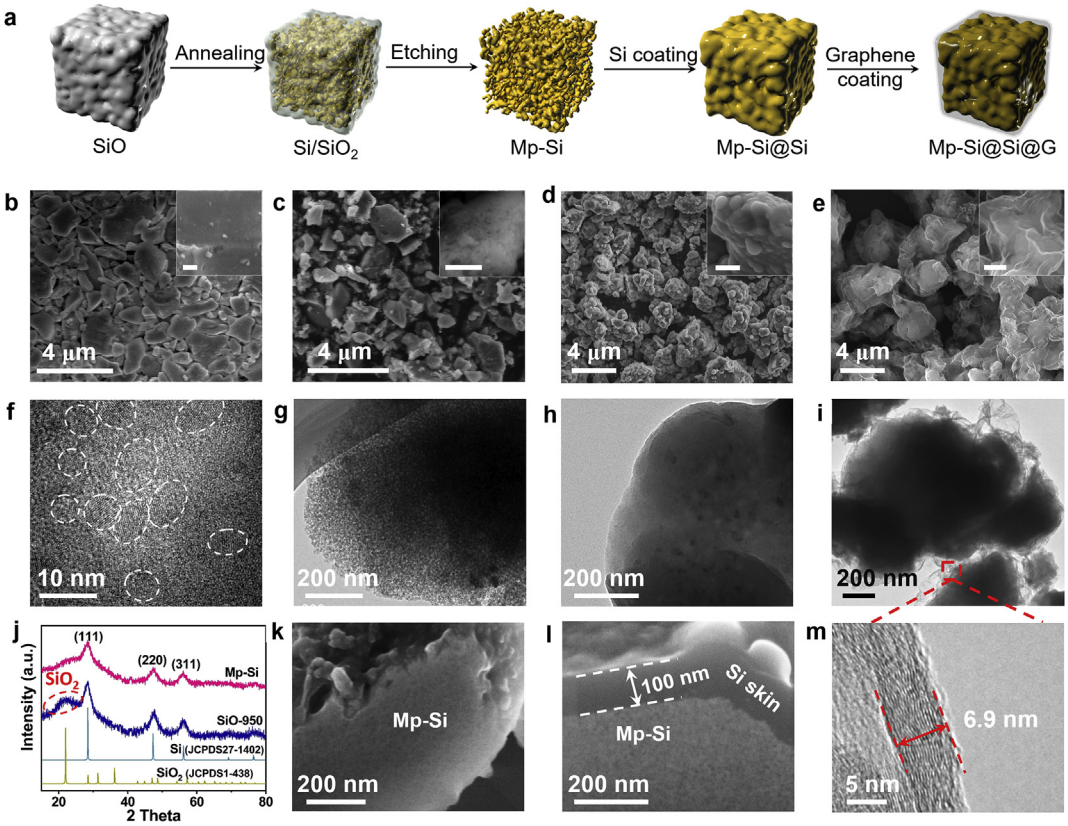

Fig. 2. Fabrication and Characterization. **a,** schematic of the fabrication process of Mp-Si@Si@G microparticles. SEM (**b-e**) and TEM (**f-i**) images of annealing-treated SiO microparticles (**b,f**), Mp-Si microparticles (**c,g**), Mp-Si@Si microparticles (**d,h**), and Mp-Si@Si@G microparticles (**e,i**). Insets are magnified SEM images showing the surface of the microparticles, scale bar is 500 nm **j,** XRD patterns of annealing-treated SiO microparticles before and after HF-etching treatment. **k,l,** FIB-SEM characterization of Mp-Si microparticles without (**k**) and with (**l**) Si-sealing. **m,** high-resolution TEM image of the graphene cage's layered structure.

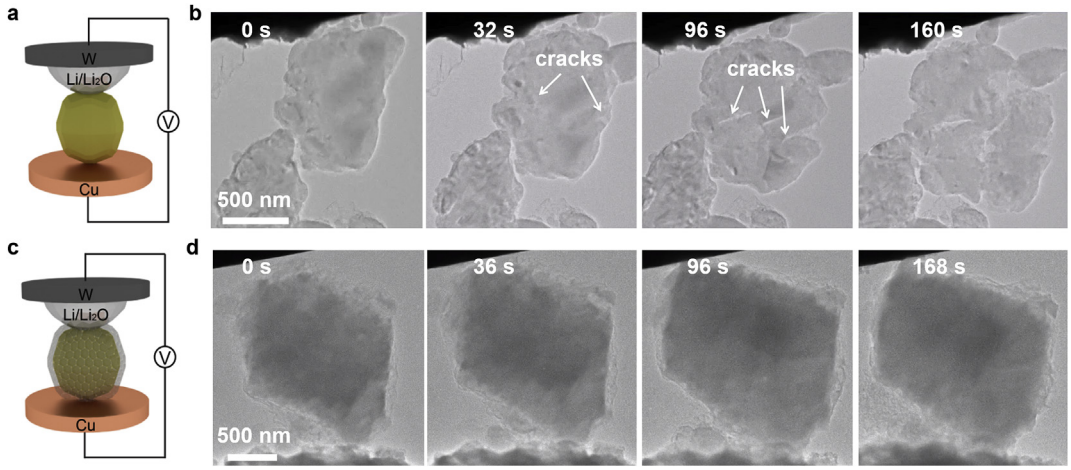

Fig. 3. *In situ* TEM characterization during lithiation. a,c, schematic of the *in situ* TEM device. **b,d,** time-lapse images of the lithiation of dense Si microparticles (see Supplementary Movie 1) and Mp-Si@Si@G microparticle (see Supplementary Movie 2). **b,** for dense Si microparticles, the Si structures fractured violently due to the huge volume expansion, and the fractured pieces scattered and lost contact from each other. **d,** for Mp-Si@Si@G microparticle, the Si structure remains robust because the inner pores can provide sufficient space to accommodate the expansion. During the whole lithiation process, the Si microparticles stay within the mechanically strong graphene cage, which remains intact throughout the highly anisotropic process.

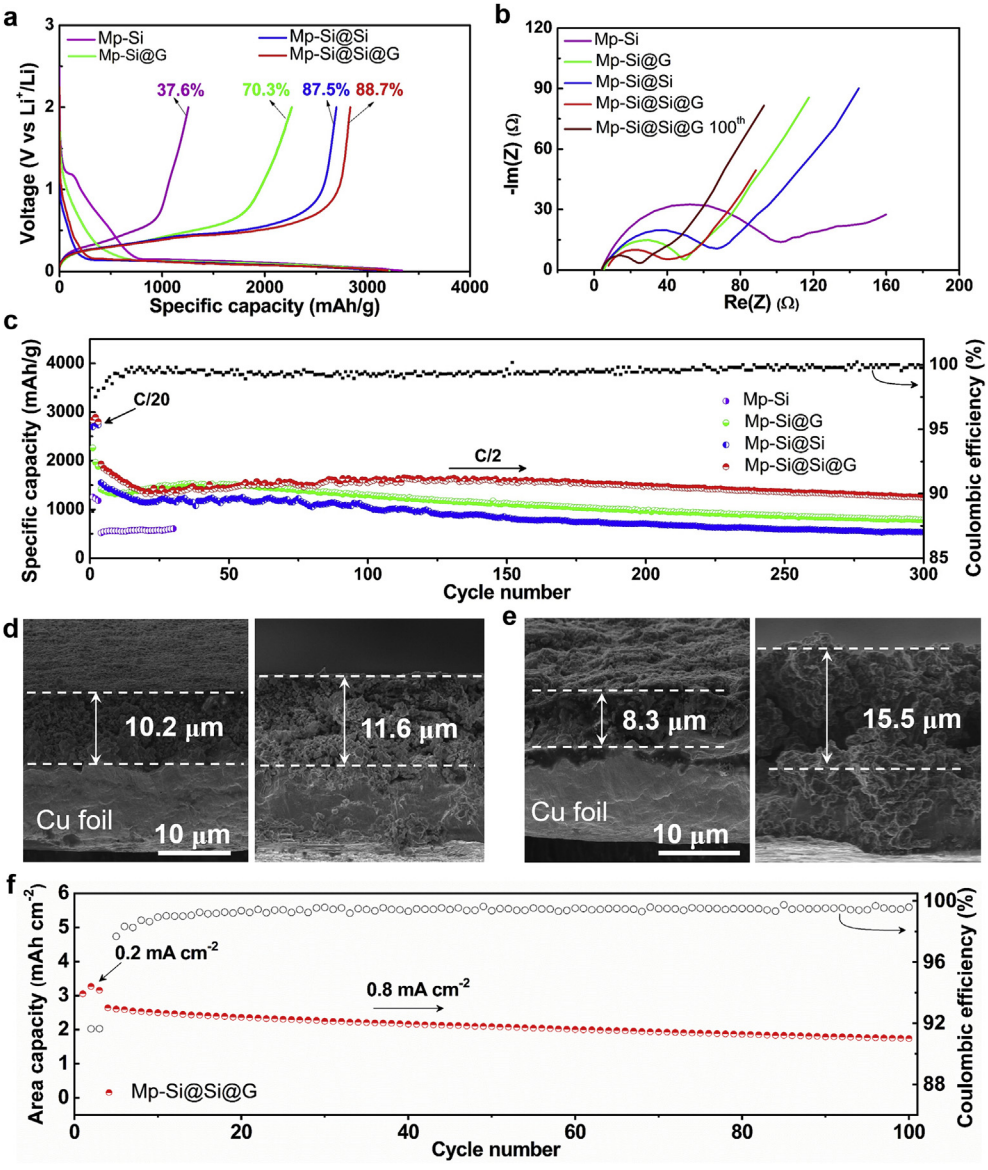

Fig. 4. Electrochemical characterization. All the specific capacities are reported based on the total mass of the active materials (Si and C in the Mp-Si@G and Mp-Si@Si@G). **a,** first-cycle voltage profiles of individual cells with corresponding Coulombic efficiencies. **b,** AC impedance spectra of as-produced Si microparticle electrodes for the 1st cycle. To better evaluate the electrochemical performance of Mp-Si@Si@G microparticles, AC impedance spectra for the 100th cycle was also tested. Electrochemical impedance spectroscopy (EIS) was carried out at a voltage of 1.0 V vs Li^+/Li. **c,** Half-cell delithiation capacity of Mp-Si with different surface-engineering treatment. For Mp-Si@G and Mp-Si@Si@G samples, no conductive additives were added. For bare Mp-Si and Mp-Si@Si samples, super P was added as a conductive additive. The mass loading of active material was around 0.68 mg cm^{-2}. The rate was C/20 for the initial three cycles and C/2 for later cycles ($1C = 4.2\,A\,g^{-1}$). The Coulombic efficiency of the Mp-Si@Si@G is plotted on the secondary y-axis. (**d,e**) Cross-sectional SEM images of Mp-Si@Si (d) and Mp-Si@Si@G (e) electrodes before (left) and after (right) cycling test. **f,** full-cell delithiation (with regard to Si) capacity of Mp-Si@Si@G microparticles paired with a traditional lithium cobalt oxide cathode. The Coulombic efficiency of the Mp-Si@Si@G microparticles is plotted on the secondary y-axis.

irreversible reactions between Li and large amount of surficial SiO_x [31,32] formed during the slurry preparation process (Fig. S11) is observed; conversely, no obvious cathodic peak indicating irreversible reactions can be observed for the Mp-Si@Si sample. Moreover, a plateau at 1.2 V ascribed to the lithiation of SiO_x is only observed for the Mp-Si sample (Fig. 4a), further indicating the highly decreased irreversible Li-consumption by surficial Si-sealing. In addition, compared to amorphous carbon coatings, the highly graphitized carbon of the graphene cage is unlikely to trap Li.

Secondly, the encapsulation of Mp-Si@Si with elastic graphene cages guarantees the formation of a stable electrode/electrolyte interface and prevents uncontrolled SEI formation. Electrochemical impedance spectroscopy (EIS) test shows that Mp-Si@Si@G microparticle electrode exhibits the smallest resistance among all electrodes after the 1st cycle (Fig. 4b), which may be due to the optimized specific surface area of Mp-Si@Si@G decreases the electrolyte accessible area, thus reducing SEI formation and irreversible Li-consumption. Besides, it's worth noting that the charge transfer resistance of Mp-Si@Si@G sample only slightly reduces after the 100th cycle, indicating that the SEI layer remains stable during the repeated cycling, enabling high later-cycle Coulombic efficiencies (Figs. 4c and 99.8–100.0%).

Besides the Coulombic efficiency, the specific capacity and cycling stability are another two most important parameters for a practical battery. The half-cell data in Fig. 4c shows that the Mp-Si@Si@G microparticles reached an initial reversible capacity of about 2834 mAh g^{-1} at a current density of C/20 (1C = 4.2 A g^{-1}). Given that the mass ratio of Si in the composite is 92%, the specific capacity normalized to Si is as high as 3080 mAh g^{-1}. The high capacity indicates that the active materials are electrically well connected and participate fully in the electrochemical lithiation and delithiation process. Note that, this is achieved without the use of any conductive additives, enabled by the excellent electrical conductivity of the graphene cage. Furthermore, a specific capacity of about 1246 mAh g^{-1} was maintained after 300 consecutive cycles at a higher rate of C/2, which is still over three times as large as that of the commercial graphite anodes' theoretical capacity and far surpasses that of Mp-Si (560 mAh g^{-1} at the 10th cycle), Mp-Si@G (792 mAh g^{-1} at the 300th cycle) or Mp-Si@Si (1047 mAh g^{-1} at the 100th cycle, 534 mAh g^{-1} at the 300th cycle). While the cycling stability of Mp-Si@Si microparticles is much better than that of dense Si microparticles (below 370 mAh g^{-1} in 20 cycles) [23], owing to the inner pore space buffering the volume expansion during the lithiation process, the SEI at the surface of Mp-Si@Si is nevertheless unstasble, resulting in poor stability in later cycles.

The exceptional electrochemical stability can be attributed to the hierarchical micro-/nanoscale architecture of the Si—C composite electrode. The void space generated during the thermal disproportionation and etching process retains secondary particles and buffers volume expansion. According to the chemical equation (1)

$$2SiO \rightarrow Si + SiO_2 \quad (1)$$

1.00 cm^3 of SiO will generate 0.30 cm^3 of Si and 0.55 cm^3 of SiO_2 after thermal disproportionation based on their density (2.1, 2.3, and 2.6 g cm^{-3} for SiO, Si, and SiO_2, respectively), which suggests a large void:Si ratio of about 11:6 was reached after SiO_2 removal. This large volume ratio allows for free volume expansion of Si material without breaking the graphene shell.

To better understand the reason for such a good cycling stability, post-cycling cross-sectional SEM analyses was carried out to show the morphology change of the Si—C composite electrode after charge/discharge. Based on the electrode thickness before and after lithiation (Fig. 4d and e), the volume expansion of the Mp-Si@Si@G microparticle electrode is calculated to be only 13.7%, which is far less than that of Mp-Si@Si microparticles (~86.7%) and dense Si microparticle (over 150%) [23], which leads to improved cycling stability.

The Mp-Si@Si@G microparticles simultaneously exhibit high Coulombic efficiency and good cycling stability (Supplementary Table 1); thus, we are able to construct a practical full-cell battery with high mass loading and improved cycling performance. In contrast to the nearly unlimited Li supply in half cells, full cells have a finite Li supply, therefore low early-cycle Coulombic efficiencies mean large irreversible Li-consumption and decreased energy density. As a result, reaching high early-cycle Coulombic efficiency is extremely critical to the cycling stability of a full cell. Furthermore, good cycling stability with a high mass loading is challenging to achieve due to the tortuous charge transfer from the current collector and larger overall volume change. In our case, good cycling stability for Mp-Si@Si@G microparticles can still be achieved when the mass loading is as high as ~2.0 mg cm^{-2} (see Figs. S12 and S13), showing great promise for practical full cell applications.

As Fig. 4f shows, when paired with a traditional lithium cobalt oxide (LCO) cathode, the Mp-Si@Si@G microparticles exhibit stable cycling (1.75 mAh cm^{-2} remained after 100 cycles) and high Coulombic efficiency at a current density of 0.8 mA cm^{-2}. Moreover, the voltage profiles at various cycle numbers (Fig. S14) show stable overpotentials, indicating that both the anode and cathode are stable during cycling. This excellent full-cell capacity and stability for microscale Si anode materials demonstrates the great promise of our surface-engineering approach in addressing the existing challenges in today's LIBs industry.

5. Conclusion

In summary, we demonstrate a surface-engineering strategy to construct hierarchical Si microstructures as high-Coulombic-efficiency anode materials for next-generation lithium-ion batteries. By sealing a mesoporous Si microparticle with a dense Si skin and further encapsulating with a graphene cage, the issues of low Coulombic efficiency, material fracture, and poor SEI stability are addressed simultaneously as demonstrated both in half cells and full cells. The Si skin lowers the electrode/electrolyte contact area and minimizes side reactions, thus leading to an initial Coulombic efficiency over two times as high as that without coating. The graphene-encapsulation, combined with the void space of the mesoporous Si core for volume expansion, maintains the structural integrity of the particle and prevents continuous SEI formation, resulting in high later-cycle Coulombic efficiencies and impressive cycling stability. In addition, the material synthesis is scalable and highly reproducible. We anticipate our surface-engineering on porous structure method may open an effective route to make high performance lithium battery anodes.

Author contributions

J.W., L.L. and Y.C. conceived and designed the experiments. J.W. and L.L. carried out materials synthesis and electrochemical characterization. J.Z., H.L. and F.S. participated in part of the synthesis and materials characterization. H.L. conducted *in situ* TEM lithiation test. J.W., L.L. and Y.C. co-wrote the paper. All authors discussed the results and commented on the manuscript.

Conflicts of interest

The authors declare no competing financial interests.

Acknowledgements

Y.C. acknowledges the support from the Assistant Secretary for Energy Efficiency and Renewable Energy, Office of Vehicle Technologies of the US Department of Energy under the Battery Materials Research (BMR) Program.

Appendix A. Supplementary data

Supplementary data to this article can be found online at https://doi.org/10.1016/j.nanoen.2019.04.070.

References

[1] A.S. Aricò, P. Bruce, B. Scrosati, J.-M. Tarascon, W. van Schalkwijk, Nanostructured materials for advanced energy conversion and storage devices, Nat. Mater. 4 (2005) 366–377.
[2] M. Armand, J.-M. Tarascon, Building better batteries, Nature 451 (2008) 652–657.
[3] P.G. Bruce, S.A. Freunberger, L.J. Hardwick, J.-M. Tarascon, Li-O_2 and Li-S batteries with high energy storage, Nat. Mater. 11 (2012) 19–29.
[4] B. Dunn, H. Kamath, J.-M. Tarascon, Electrical energy storage for the grid: a battery of choices, Science 334 (2011) 928–935.
[5] J. Wang, H. Tang, L. Zhang, H. Ren, R. Yu, Q. Jin, J. Qi, D. Mao, M. Yang, Y. Wang, P. Liu, Y. Zhang, Y. Wen, L. Gu, G. Ma, Z. Su, Z. Tang, H. Zhao, D. Wang, Multi-shelled metal oxides prepared via an anion-adsorption mechanism for lithium-ion batteries, Nature Energy 1 (2016) 15050.
[6] F. Shi, Z. Song, P.N. Ross, G.A. Somorjai, R.O. Richie, K. Komvopoulos, Failure mechanisms of single-crystal Si electrodes in lithium-ion batteries, Nat. Commun. 7 (2016) 11886.
[7] Y.M. Sun, N. Liu, Y. Cui, Promises and challenges of nanomaterials for lithium-based rechargeable batteries, Nature Energy 1 (2016) 16071.
[8] L.-F. Cui, R. Ruo, C.K. Chan, H. Peng, Y. Cui, Crystalline-amorphous core-shell Si nanowires for high capacity and high current battery electrodes, Nano Lett. 9 (2008) 491–495.
[9] Y. Xiao, D. Hao, H. Chen, Z. Gong, Y. Yang, Economical synthesis and promotion of the electrochemical performance of silicon nanowires as anode material in Li-ion batteries, ACS Appl. Mater. Interfaces 5 (2013) 1681–1687.
[10] S. Zhou, X. Liu, D. Wang, Si/$TiSi_2$ heteronanostructures as high-capacity anode material for Li ion batteries, Nano Lett. 10 (2010) 860–863.
[11] Y. Zhou, X. Jiang, L. Chen, J. Yue, H. Xu, J. Yang, Y. Qian, Novel mesoporous silicon nanorod as an anode material for lithium ion batteries, Electrochim. Acta 127 (2014) 252–258.
[12] S. Soleimani-Amiri, S.A.S. Tali, S. Azimi, Z. Sanaee, S. Mohajerzadeh, Highly featured amorphous silicon nanorod arrays for high-performance lithium-ion batteries, Appl. Phys. Lett. 105 (2014) 193903.
[13] J. Xiao, W. Xu, D. Wang, D. Choi, W. Wang, X. Li, G.L. Graff, J. Liu, J.-G. Zhang, Stabilization of Si anode for Li-ion batteries, J. Electrochem. Soc. 157 (2010) A1047–A1051.
[14] M. Ge, J. Rong, X. Fang, C. Zhou, Porous doped Si nanowires for lithium ion battery anode with long cycle life, Nano Lett. 12 (2012) 2318–2323.
[15] R. Yi, F. Dai, M.L. Gordin, S. Chen, D. Wang, Micro-sized Si-C composite with interconnected nanoscale building blocks as high-performance anodes for practical application in lithium-ion batteries, Adv. Energy Mater. 3 (2013) 295–300.
[16] A. Magasinski, P. Dixon, B. Hertzberg, A. Kvit, J. Ayala, G. Yushin, High-performance lithium-ion anodes using a hierarchical bottom-up approach, Nat. Mater. 9 (2010) 353–358.
[17] L. Ji, H. Zheng, A. Ismach, Z. Tan, S. Xun, E. Lin, V. Battaglia, V. Srinivasan, Y. Zhang, Graphene/Si multilayer structure anodes for advanced half and full lithium-ion cells, Nanomater. Energy 1 (2012) 164–171.
[18] I.H. Son, J.H. Park, S. Kwon, S. Park, M.H. Rummeli, A. Bachmatiuk, H.J. Song, J. Ku, J.W. Choi, J. Choi, S.G. Doo, H. Chang, Si carbide-free graphene growth on Si for lithium-ion battery with high volumetric energy density, Nat. Commun. 6 (2015) 7393.
[19] Y. Yao, M.T. McDowell, I. Ryu, H. Wu, N. Liu, L. Hu, W.D. Nix, Y. Cui, Interconnected Si hollow nanospheres for lithium-ion battery anodes with long cycle life, Nano Lett. 11 (2011) 2949–2954.
[20] M.-H. Park, M.G. Kim, J. Joo, K. Kim, J. Kim, S. Ahn, Y. Cui, J. Choi, Si nanotube battery anodes, Nano Lett. 9 (2009) 3844–3847.
[21] H. Wu, G. Chan, J.W. Choi, I. Ryu, Y. Yao, M.T. McDowell, S.W. Lee, A. Jackson, Y. Yang, L. Hu, Y. Cui, Stable cycling of double-walled Si nanotube battery anodes through solid-electrolyte interphase control, Nat. Nanotechnol. 7 (2012) 310–315.
[22] N. Liu, H. Wu, M.T. McDowell, Y. Yao, C. Wang, Y. Cui, A yolk-shell design for stabilized and scalable Li-ion battery alloy anodes, Nano Lett. 12 (2012) 3315–3321.
[23] Y. Li, K. Yan, H.-W. Lee, Z. Lu, N. Liu, Y. Cui, Growth of conformal graphene cages on micrometre-sized Si particles as stable battery anodes, Nature Energy 1 (2016) 15029.
[24] N. Liu, Z. Lu, J. Zhao, M.T. McDowell, H.-W. Lee, W. Zhao, Y. Cui, A pomegranate-inspired nanoscale design for large-volume-change lithium battery anodes, Nat. Nanotechnol. 9 (2014) 187–192.
[25] Z. Lu, N. Liu, H.-W. Lee, J. Zhao, W. Li, Y. Li, Y. Cui, Nonfilling carbon coating of porous Si micrometer-sized particles for high-performance lithium battery anodes, ACS Nano 9 (2015) 2540–2547.
[26] M. Mamiya, M. Kikuchi, H. Takei, Crystallization of fine Si particles from Si monoxide, J. Cryst. Growth 237 (2002) 1909–1914.
[27] S. Nagakura, Study of metallic carbides by electron diffraction part I. Formation and decomposition of nickel carbide, J. Phys. Soc. Jpn. 12 (1957) 482–494.
[28] S.-M. Yoon, W.M. Choi, H. Baik, H.-J. Shin, I. Song, M.-S. Kwon, J.J. Bae, H. Kim, Y.H. Lee, J.-Y. Choi, Synthesis of multilayer graphene balls by carbon segregation from nickel nanoparticles, ACS Nano 6 (2012) 6803–6811.
[29] X. Li, W. Cai, L. Colombo, R.S. Ruo, Evolution of graphene growth on Ni and Cu by carbon isotope labeling, Nano Lett. 9 (2009) 4268–4272.
[30] D.J. Xue, S. Xin, Y. Yan, K.-C. Jiang, Y.-X. Yin, Y.-G. Guo, L.-J. Wan, Improving the electrode performance of Ge through Ge@C Core – Shell nanoparticles and graphene networks, J. Am. Chem. Soc. 134 (2012) 2512–2515.
[31] N. Yan, F. Wang, H. Zhong, Y. Li, Y. Wang, L. Hu, Q. Chen, Hollow porous SiO_2 nanocubes towards high-performance anodes for lithium-ion batteries, Sci. Rep. 3 (2013) 1568.
[32] R. Lv, J. Wang, J. Wang, Y. NuLi, Electrodeposited porous-microspheres Li–Si films as negative electrodes in lithium-ion batteries, J. Power Sources 196 (2011) 3868–3873.

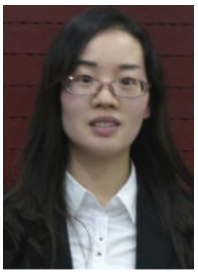

Jiangyan Wang received her PhD from the institute of Process Engineering, Chinese Academy of Sciences. She is currently a postdoctoral scholar at Stanford University. Her current research interests are focused on the design and synthesis of micro- /nano-structured materials and nano-materials for energy conversion and storage.

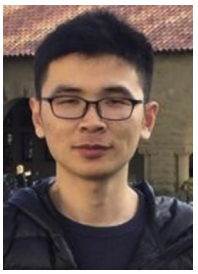

Lei Liao received his BS degree and PhD from Peking University and worked as a postdoctoral scholar at Stanford University. He is currently a scientist at 4C Air, a start-up company focusing on the air filtration.

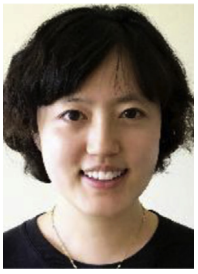

Hye Ryoung Lee received her PhD from the Department of Electrical Engineering at Stanford University. She is currently a staff scientist at Stanford University. Her research interests are nanoscale materials and their application on wearable energy/electronic devices.

Feifei Shi received her PhD from the University of California, Berkeley. She is currently a postdoctoral scholar at Stanford University. Her research interests focuse on electrochemical and mechanical processes at surfaces and interfaces of advanced materials for energy storage.

William Huang received his BS in Nanoengineering from the University of California, San Diego and is currently a PhD candidate in Materials Science and Engineering at Stanford University. His research focuses on cryogenic-electron microscopy of battery materials.

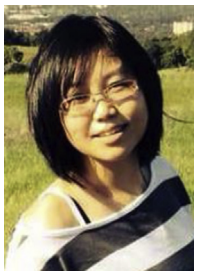

Jie Zhao received her PhD from the Department of Materials Science and Engineering at Stanford University. She is currently a postdoctoral scholar at Northwestern University. Her research focuses on nanomaterials for energy storage and bioelectronics.

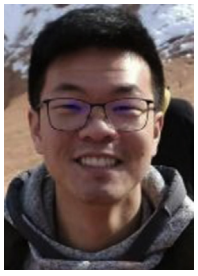

Allen Pei received his BS from the University of California, San Diego and is currently a PhD candidate in Materials Science and Engineering at Stanford University. His research focuses on nanomaterials for energy storage, fundamental mechanism study and characterization methods development.

Jing Tang received her PhD from Fudan University and worked as a postdoctoral scholar at Harvard University. She is currently a postdoctoral scholar at Stanford University. Her research focuses on nanomaterials design and synthesis for catalysis.

Xueli Zheng received her PhD from Tianjin University and was educated as a visiting student at University of Toronto. She is currently a postdoctoral scholar at Stanford University. Her research focuses on nanomaterials design and synthesis for catalysis.

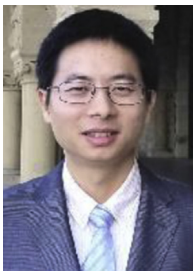

Wei Chen received his PhD from King Abdullah University of Science and Technology (KAUST) He is currently a postdoctoral scholar at Stanford University. His research focuses on grid-scale energy storage and electrocatalysis.

Yi Cui is a professor at Stanford University and SLAC National Accelerator Laboratory. He received his B.S. from the University of Science and Technology of China in 1998 and his Ph.D. from Harvard University in 2002. He was a Miller Postdoctoral Fellow at the University of California, Berkeley and joined in Stanford as a faculty member in 2005. His current research is on nanomaterials design for energy and environment. He is a co-director of the Bay Area Photovoltaic Consortium and Battery 500 Consortium.